Backward waves with double zero-group-velocity points in a liquid-filled pipe

Hanyin Cui,[a] Weijun Lin, Hailan Zhang, and Xiuming Wang
State Key Laboratory of Acoustics, Institute of Acoustics, Chinese Academy of Sciences, Beijing 100190, People's Republic of China

Jon Trevelyan
School of Engineering and Computing Sciences, Durham University, Durham DH1 3LE, United Kingdom

(Received 12 August 2015; revised 18 February 2016; accepted 2 March 2016; published online 17 March 2016)

Hollow cylinders often exhibit backward propagation modes whose group and phase velocities have opposite directions, and these exhibit a minimum possible frequency at which the group velocity vanishes at a nonzero wavenumber. These zero-group-velocity (ZGV) points are associated with resonant conditions in the medium. On the basis of ZGV resonances, a non-contact and laser ultrasound technique has been developed to measure elastic constants of hollow pipes. This paper provides a theoretical and numerical investigation of the influence of the contained liquid on backward waves and associated ZGV modes, in order to explore whether this ZGV technique is suitable for in-service non-destructive evaluations of liquid-filled pipes. Dispersion spectra and excitation properties have been analyzed. It is found that the presence of the liquid causes an increased number of backward modes and ZGVs which are highly excitable by a point source. In addition, several guided modes twice undergo a change of sign in the slopes of their dispersion curves, leading to two ZGV points. This phenomenon of double ZGVs in one backward wave, which is caused by strong mode repulsions, has not been found in isotropic hollow cylinders, but it can be observed in a fluid-filled thin-walled pipe.
 [http://dx.doi.org/10.1121/1.4944046]

[ANN] Pages: 1179–1194

I. INTRODUCTION

In the frequency-wavenumber ($\omega - k$) spectra, a dispersion curve of a guided wave may exhibit a portion of negative slope, where the group and phase velocities are directed in the opposite directions. This phenomenon is termed "backward wave propagation"[1–3] or "negative group velocity."[4–7] A related phenomenon is the zero-group-velocity (ZGV) point where the slope changes sign, that is, the group velocity vanishes at a nonzero wavenumber.[8,9] At these ZGV points, the acoustic energy of the corresponding ZGV modes is trapped in the source area without any transfer to the adjacent medium. The resulting resonance is sensitive to local mechanical properties and dimensional changes of isotropic and anisotropic materials.[10–12] Recently, laser excitation and detection of such ZGV modes has attracted considerable attention with the prospect of the application of this phenomenon to measure elastic constants and structural defects of thin plates,[9,12–16] hollow cylinders,[13,17] solid transversely isotropic (TI) cylinder,[18] and supported thin film structures (i.e., multilayered plane structures).[19–21]

Liquid-filled pipes used in the civil and energy industries need to be inspected regularly to certify their safety and reliability.[22] For hollow cylinders, a non-contact, laser ultrasonic technique based on ZGV Lamb modes has been developed for non-destructive evaluation application.[13,17] The objective of this work is to study the effect of a contained liquid on backward waves and the associated ZGV modes, and thereby to investigate whether this ZGV technique can be used for in-service inspection of liquid transportation pipelines.

The existence of backward wave and ZGV points in elastic plates and cylinders has been recognized for more than one century. As early as 1904, Lamb[23] first discussed the possibility of backward wave propagation. In 1957, Tolstoy and Usdin[24] predicted the existence of the backward mode S_{2b} in a free isotropic plate with Poisson's ratio of 0.25. The subscript b denotes backward wave. Mindlin[8] and Mindlin and Medick[25] numerically plotted the complex frequency-wavenumber spectra of Lamb waves in plates having Poisson's ratios less than, equal to, and greater than the special case of $\nu = 1/3$. In these $\omega - k$ spectra, backward propagation branches with negative slopes are clearly identified in the vicinity of wavenumber $k = 0$. Furthermore, each backward branch possesses only one ZGV point that has been observed at the saddle point with a horizontal slope.

In addition, considerable experimental evidence of backward waves and ZGV modes has been reported.[1–5,9–19,21,26,27] For instance, Zemanek[28] has made the observation of a ZGV resonance of the low-order, longitudinal guided mode in a free rod. Meitzler[1] reported experimental observations of stress pulses travelling in backward elastic-wave motions in

[a]Electronic mail: cuihanyin@mail.ioa.ac.cn

cylinders and plates. Negishi[4] and Negishi and Li[29] reported the "negative group velocity" phenomenon of Lamb waves in S_1 and A_2 modes.

More recently, it has become possible to use computationally intensive numerical procedures to gain an improved understanding of backward waves and ZGVs in various waveguides. Most researchers have focused on the discussions of isotropic plates, anisotropic plates, and multilayered structures. For the case of an isotropic plate, in 1987, Negishi[30] revealed that the existence of backward wave depends on Poisson's ratio. In addition, in 2008, Prada *et al.*[14] numerically analyzed the existence conditions of ZGV-Lamb modes as determined by the value of Poisson's ratio, and concluded that all Lamb modes, with the exception of the three lowest ones, can exhibit ZGV modes. Moreover, they found that, a strong repulsion between a pair of symmetric (or antisymmetric) Lamb modes having a different parity in the vicinity of their cutoff frequencies may cause the existence of a backward wave and the associated ZGV point. In 2009, Prada *et al.*[12] expanded their ZGV research to anisotropic material and observed the so called S_1-ZGV and A_2-ZGV modes of a silicon plate with cubic symmetry. In 2012, Hussain and Ahmad[31] reported the multiple ZGV points of Lamb modes in an orthotropic plate (iodic acid). For multilayered structures, Maznev and Every[19,20] analyzed the existence of backward propagating acoustic waves in supported layers, and experimentally proved that the lowest mode of a supported thin film structure could exhibit the phenomenon of "negative group velocity" and double ZGV points. Furthermore, in 2012, Kausel[32] theoretically analyzed the number and location of ZGV modes in horizontally layered media bounded by any arbitrary combination of external boundaries, and concluded that the effective number of ZGVs is small and decreases as Poisson's ratio increases.

Guided elastic waves in cylindrical structures also exhibit backward waves and ZGVs. Marston[33] and Kaduchak *et al.*[34] discussed the effect of backward wave propagation on the scattering of sound by shells. Ces *et al.*[17] investigated the ZGV resonances in a Zircaloy hollow cylinder by laser based ultrasonic techniques, in order to deduce the elastic constants. For elastic plates, backward Lamb waves depend only on Poisson's ratio;[14] while, for hollow pipes, backward waves also depend on the ratio of the inner to the outer radius.[35] Cui *et al.*[35] numerically studied the influence of the radius ratio on group velocities of backward waves in hollow cylinders.

As reviewed in the above paragraphs, the existence conditions and dispersion properties of backward waves and the associated ZGVs in plates, hollow cylinders, and multilayered structures have been extensively investigated. There are also a lot of works about the propagation of guided waves in liquid-filled pipes.[22,36,37] However, it seems that the dispersion and excitation properties of backward waves and ZGVs in liquid-filled pipes have not been reported.

In this paper, theoretical and numerical results for liquid-filled pipes are presented with specific attention paid to the excitation characteristics of ZGV modes. Dispersion curves and amplitude spectra have been analyzed in order to study the influence of the contained liquid on backward waves and ZGVs in pipes with different ratios of the inner to the outer radius. Moreover, it is shown that, in addition to the backward modes with a single ZGV point, there are several modes which possess two ZGV points. This phenomenon of multiple ZGVs has been reported only in three kinds of waveguides, i.e., supported thin film structures,[19] orthotropic plates,[31] and multilayered pipes.[38] We introduce a mode coupling effect to interpret the existence of the double-ZGVs.

II. THEORY

A. Dispersion equation for axisymmetric modes

In this section, a brief review of the development of the dispersion equation for axisymmetric modes with the circumferential number $n=0$ in a liquid-filled pipe is summarized.[39–43] The considered model of interest is a circular pipe filled with an inviscid liquid in the cylindrical coordinates (r, z, θ), where the z-axis is along the symmetric axis of the pipe. The length of the pipe is assumed to be infinite, and the internal and external radii of the pipe are denoted a and b, respectively. The wall-thickness of the pipe is $d = b - a$. The longitudinal bulk velocity and density of the liquid are denoted V_f and ρ_1, while the longitudinal and shear bulk velocities and density of the solid pipe are denoted V_L, V_T, and ρ_2, respectively.

In the frequency-wavenumber $(\omega - k)$ domain, in the absence of body forces, the displacement potential function of the compressional wave in the liquid contained in the cylinder can be expressed as[44]

$$\phi_1 = A_1 I_0(\alpha_1 r), \tag{1}$$

where the (exponential) propagative term, $\exp(ikz - i\omega t)$, is omitted for convenience in the scalar and the vector potentials (fluid and solid). Displacement potential functions of the compressional (P), shear vertical (SV), and shear horizontal (SH) waves in the pipe are[44]

$$\begin{aligned} \phi_2 &= A_2 I_0(\alpha_2 r) + B_2 K_0(\alpha_2 r), \\ \psi_2 &= C_2 I_0(\beta_2 r) + D_2 K_0(\beta_2 r), \\ \chi_2 &= 0, \end{aligned} \tag{2}$$

where $I_0(x)$ and $K_0(x)$ are modified Bessel functions of the first and second kind, and A_1, A_2, B_2, C_2, D_2 are the unknown coefficients to be determined by consideration of the boundary conditions. The other parameters in Eqs. (1) and (2) are

$$\alpha_1 = \sqrt{k^2 - k_f^2}, \quad \alpha_2 = \sqrt{k^2 - k_L^2}, \quad \beta_2 = \sqrt{k^2 - k_T^2}, \tag{3}$$

where wavenumbers of longitudinal and shear bulk waves in the liquid and pipe are

$$k_f = \omega/V_f, \quad k_L = \omega/V_L, \quad k_T = \omega/V_T, \tag{4}$$

and the wavenumber of the guided wave propagating along the z-axis is

$$k = \omega/V, \tag{5}$$

where ω is the angular frequency, and V is the phase velocity of the guided wave.

The modified Bessel functions $I_0(x)$ and $K_0(x)$ in the displacement potentials (1) and (2) are replaced by the unmodified Bessel functions $J_0(ix)$ and $Y_0(ix)$ when the argument x is purely imaginary. This choice of Bessel functions leads to a more stable solution of the dispersion equation.[45,46] Two functions $P_0(x)$ and $Q_0(x)$ are employed in the rest of the derivation to represent Bessel functions, which are

$$P_0(x) = \begin{cases} I_0(x), & \text{for real } x \\ J_0(ix), & \text{for imaginary } x, \end{cases}$$
$$Q_0(x) = \begin{cases} K_0(x), & \text{for real } x \\ Y_0(ix), & \text{for imaginary } x. \end{cases} \tag{6}$$

The liquid-solid interface conditions are that the radial displacement and normal stress components at the boundary are continuous, and the shear stress components are zero at the interface. That is, the boundary conditions at $r = a$ are

$$\begin{aligned} &u_{r,1}|_{r=a} = u_{r,2}|_{r=a}, \\ &\sigma_{rr,1}|_{r=a} = \sigma_{rr,2}|_{r=a}, \\ &\sigma_{rz,2}|_{r=a} = 0. \end{aligned} \tag{7}$$

It is further assumed that the pipe is surrounded by a vacuum. Thus, on the outer surface of the pipe is traction free, i.e., the boundary conditions at $r = b$ can be written as

$$\sigma_{rr,2}|_{r=b} = \sigma_{rz,2}|_{r=b} = 0. \tag{8}$$

The *Helmholtz* decomposition is applied. The displacement and stress components in the liquid and the pipe can be obtained by substituting the displacement potentials (1) and (2) into the constitutive equations, respectively. Then, application of the boundary conditions (7) and (8) yields five homogeneous equations with five unknown coefficients. The determinant of the matrix expressing these equations must vanish for a nontrivial solution to exist. This produces the dispersion equation in the form of

$$\begin{aligned} \Delta &= \begin{vmatrix} M_{11} & M_{12} & M_{13} & M_{14} & M_{15} \\ M_{21} & M_{22} & M_{23} & M_{24} & M_{25} \\ 0 & M_{32} & M_{33} & M_{34} & M_{35} \\ 0 & M_{42} & M_{43} & M_{44} & M_{45} \\ 0 & M_{52} & M_{53} & M_{54} & M_{55} \end{vmatrix} \\ &= |M_{ij}(V_f, \rho_1, V_L, V_T, \rho_2, \omega, k)| = 0 \quad (i,j = 1,2,...,5), \end{aligned} \tag{9}$$

where the matrix elements are given in the Appendix. The bisection technique[46] has been used to numerically solve the transcendental Eq. (9) to yield the real roots of the dispersion equation (i.e., phase velocities of non-leaky guided modes). The bisection technique is good at robustly finding the real branches of the dispersion equation without initial-guess of the root. And it is stable when two roots are in close proximity.[46] However, it converges slower compared to Newton-Raphson or Muller zero-finding algorithm.[47] For large radius pipes (i.e., the large *fd* problem), it is recommended using Newton-Raphson method or Muller zero-finding algorithm.

B. Mode coupling

The dispersion Eq. (9) of axisymmetric guided modes in the liquid-filled pipe can be expressed as the superposition of two terms,

$$\begin{aligned} \Delta = M_{11} &\begin{vmatrix} M_{22} & M_{32} & M_{42} & M_{52} \\ M_{23} & M_{33} & M_{43} & M_{53} \\ M_{24} & M_{34} & M_{44} & M_{54} \\ M_{25} & M_{35} & M_{45} & M_{55} \end{vmatrix} \\ - M_{21} &\begin{vmatrix} M_{12} & M_{32} & M_{42} & M_{52} \\ M_{13} & M_{33} & M_{43} & M_{53} \\ M_{14} & M_{34} & M_{44} & M_{54} \\ M_{15} & M_{35} & M_{45} & M_{55} \end{vmatrix}, \end{aligned} \tag{10}$$

where the matrix element $M_{21} = -\rho_1 a^2 \omega^2 P_0(\alpha_1 a)/\rho_2 V_T^2$. If the value of the second term of Eq. (10) is much smaller than that of the first term, the dispersion equation can be simplified. For instance, when the ratio of the density of the liquid to that of the pipe is small enough (i.e., $\rho_1/\rho_2 \to 0$), the element M_{21} and the second term both tend to zero. In this case, the dispersion Eq. (10) can be simplified as

$$\Delta \approx M_{11} \begin{vmatrix} M_{22} & M_{32} & M_{42} & M_{52} \\ M_{23} & M_{33} & M_{43} & M_{53} \\ M_{24} & M_{34} & M_{44} & M_{54} \\ M_{25} & M_{35} & M_{45} & M_{55} \end{vmatrix}. \tag{11}$$

This simplification shows that guided modes in the liquid-filled pipe can be viewed as the outcome of mode coupling between two groups of guided modes propagating in two models, respectively. These two models are two parts of the liquid-filled pipe, i.e., one model is the hypothetical liquid-cylinder with a rigid wall at $r = a$, and the other is the hollow pipe in vacuum. The reason for this conclusion is explained below.

For the hypothetical liquid-cylinder of radius a with a rigid wall *at* $r = a$, the boundary condition is that the radial component of velocity must vanish at the wall.[48] The dispersion equation of axisymmetric guided modes in this model is[48]

$$\Delta_l(V_f, \omega, k) = M_{11} = 0. \tag{12}$$

For a hollow pipe of inner and external radii a and b, respectively, in vacuum, the boundary conditions are that all the stress components are equal to zero on the inner and outer surfaces of the pipe. The dispersion equation of axisymmetric guided modes can be written as[49]

$$\Delta_p(V_L, V_T, \omega, k) = \begin{vmatrix} M_{22} & M_{32} & M_{42} & M_{52} \\ M_{23} & M_{33} & M_{43} & M_{53} \\ M_{24} & M_{34} & M_{44} & M_{54} \\ M_{25} & M_{35} & M_{45} & M_{55} \end{vmatrix} = 0. \tag{13}$$

Hence, the simplified dispersion Eq. (11) of guided modes in a liquid-filled pipe can be expressed as the product of two

dispersion Eqs. (12) and (13) governing guided modes in the liquid cylinder and in the hollow pipe, respectively. That is,

$$\Delta \approx \Delta_l(V_f, \omega, k) \cdot \Delta_p(V_L, V_T, \omega, k). \tag{14}$$

This decoupling means that guided modes in the liquid-filled pipe can be decoupled into guided modes propagating in the liquid and in the pipe, respectively.

This mode-coupling concept is helpful for understanding the existence and dispersion properties of backward waves and ZGV modes in a liquid-filled pipe. First, in a hypothetical liquid cylinder, only compressional waves exist. Since there is no repulsion between two compressional waves, neither a backward wave nor a ZGV mode exists in a liquid cylinder. Hence, all the guided modes are forward propagating modes in a liquid cylinder. Second, in a hollow pipe, it has been known that the strong repulsion between two neighboring compressional and shear waves may generate a backward wave which possesses only one ZGV point at the lowest frequency of the backward wave.[35] The existence condition and dispersion properties of backward waves and ZGVs are determined by the value of Poisson's ratio and the ratio of the inner to the outer radius of the hollow pipe.[13,17,35] Moreover, all the longitudinal modes, with the exception of the lowest one, can exhibit backward waves and ZGVs.[35] For further information on the properties of backward waves and ZGVs in a hollow pipe, the reader is referred to existing literature.[13,17,33–35] In Sec. III A, the coupling effect between the forward propagating waves in a liquid cylinder and the backward propagating waves in a hollow pipe is analyzed to study the generation of backward waves and ZGVs in a liquid-filled pipe.

C. Point source excitation

A point source is introduced in order to simulate the excitation of guided modes in the liquid-filled pipe system. We apply a spherically symmetric excitation source acting at the origin of the cylindrical coordinates, so that only longitudinal modes are excited. In the frequency-wavenumber domain, the displacement potential of the compressional wave excited by the point source is[50]

$$\phi(r, \omega, k) = \frac{X(\omega)}{4\pi^2 \rho_1 \omega^2} K_0(\alpha_1 r) = S(\omega) K_0(\alpha_1 r), \tag{15}$$

where $X(\omega)$ is the point source function. $S(\omega)$ is introduced to simplify the expressions,

$$S(\omega) = \frac{X(\omega)}{4\pi^2 \rho_1 \omega^2}. \tag{16}$$

D. Displacement component expressions

As is shown in the above section, suppose the acoustic point-source at the origin of the coordinates, the compressional displacement potential function in the liquid is[50]

$$\phi_1 = A_1 P_0(\alpha_1 r) + S(\omega) K_0(\alpha_1 r). \tag{17}$$

Substituting Eqs. (2) and (17) into Eqs. (7) and (8), yields a system of linear non-homogeneous equations, i.e.,

$$\begin{bmatrix} M_{11} & M_{12} & M_{13} & M_{14} & M_{15} \\ M_{21} & M_{22} & M_{23} & M_{24} & M_{25} \\ 0 & M_{32} & M_{33} & M_{34} & M_{35} \\ 0 & M_{42} & M_{43} & M_{44} & M_{45} \\ 0 & M_{52} & M_{53} & M_{54} & M_{55} \end{bmatrix} \cdot \begin{bmatrix} A_1/a \\ A_2/a \\ -i\beta_2 C_2/a \\ B_2/a \\ -i\beta_2 D_2/a \end{bmatrix} = \begin{bmatrix} H_1 \\ H_2 \\ 0 \\ 0 \\ 0 \end{bmatrix}, \tag{18}$$

where elements $H_1 = S(\omega)\{[dK_0(\alpha_1 r)]/dr\}$, $H_2 = -\{[S(\omega)\rho_1 a^2 \omega^2 K_0(\alpha_1 r)]/\mu_2\}$, and the other matrix elements $M_{11}, ..., M_{55}$ are listed in the Appendix.

The linear system (18) has a unique solution if and only if the determinant of the coefficient matrix of the left hand side of Eq. (18) is nontrivial, i.e., $\Delta \neq 0$. In this case, by applying Cramer's rule, the coefficients used in the expressions for displacement potentials are found to be

$$A_1 = \frac{\Delta_1 a}{\Delta}, \quad A_2 = \frac{\Delta_2 a}{\Delta}, \quad C_2 = \frac{a\Delta_3}{i\beta_2 \Delta},$$
$$B_2 = \frac{\Delta_4 a}{\Delta}, \quad D_2 = \frac{a\Delta_5}{i\beta_2 \Delta}, \tag{19}$$

where Δ is the secular equation, and Δ_l ($l = 1,2,3,4,5$) denote the determinants of the matrices obtained by replacing the lth column with the column $(H_1, H_2, 0, 0, 0)^T$ on the right hand side of Eq. (18).

Since the displacement potentials and their coefficient Eq. (19) are determined, by using the displacement potential equation[51]

$$\boldsymbol{U} = \nabla\phi + \nabla \times \nabla \times (\psi \boldsymbol{e}_z), \tag{20}$$

the solutions of the displacement components in the frequency domain is obtained. For instance, it can be shown that radial and axial displacement components $u_{r,1}, u_{z,1}$ in the inner liquid are

$$u_{r,1}(r, z, \omega) = \int_{-\infty}^{+\infty} \alpha_1 a \left[\frac{P_0'(\alpha_1 r)\Delta_1 + S(\omega)K_0'(\alpha_1 r)\Delta}{\Delta}\right] \exp(ikz) dk, \tag{21}$$

$$u_{z,1}(r, z, \omega) = \int_{-\infty}^{+\infty} -ika \left[\frac{P_0(\alpha_1 r)\Delta_1 + S(\omega)K_0(\alpha_1 r)\Delta}{\Delta}\right] \exp(ikz) dk, \tag{22}$$

and the radial and axial displacement components, $u_{r,2}, u_{z,2}$, in the pipe are

$$u_{r,2}(r, z, \omega) = \int_{-\infty}^{+\infty} [T_{I,r} + T_{K,r}] \exp(ikz) dk,$$
$$T_{I,r} = \alpha_2 a P_0'(\alpha_2 r)\frac{\Delta_2}{\Delta} + ka P_0'(\beta_2 r)\frac{\Delta_3}{\Delta},$$
$$T_{K,r} = \alpha_2 a Q_0'(\alpha_2 r)\frac{\Delta_4}{\Delta} + ka Q_0'(\beta_2 r)\frac{\Delta_5}{\Delta}, \tag{23}$$

$$u_{z,2}(r,z,\omega) = \int_{-\infty}^{+\infty} -i[T_{I,z} + T_{K,z}]\exp(ikz)dk,$$
$$T_{I,z} = kaP_0(\alpha_2 r)\frac{\Delta_2}{\Delta} + \beta_2 aP_0(\beta_2 r)\frac{\Delta_3}{\Delta},$$
$$T_{K,z} = kaQ_0(\alpha_2 r)\frac{\Delta_4}{\Delta} + \beta_2 aQ_0(\beta_2 r)\frac{\Delta_5}{\Delta}, \quad (24)$$

where $P_0'(x)$ and $Q_0'(x)$ are the first derivative of the modified (or unmodified) Bessel functions of the first and second kind of order $n=0$, respectively, which can be determined by using the recurrence relations. For longitudinal modes with $n=0$, the circumferential displacement component $u_\theta = u\sin n\theta$ is equal to zero.

Taking the radial displacement component $u_{r,1}$ for example, the complex variable Cauchy's integral formula can be applied to evaluate the integral over the wavenumber k in Eq. (21).[50] As shown in Fig. 1, in the complex plane, a closed contour of integration is constructed. It consists of the $-\infty$ to $+\infty$ integration path on the real axis, the vertical branch cuts from infinite to each of the branch points k_L, k_T, k_f, and the semicircular arc of infinite radius in the upper half of the complex k plane. The branch points correspond to wavenumbers of longitudinal and shear bulk waves in the liquid and the pipe. Since an acoustic source distributes only in a finite range, the semicircular arc of infinite radius is trivial to the integral.[50] Hence, the integral in Eq. (21) can be evaluated as the sum of the contributions due to the branch cuts and the poles. Note that the complex poles in the contour, if there exist, are ignored as only the propagating modes are taken into account in this case.

The displacement components of the guided modes can then be evaluated as 2πi times the sum of the residues of the enclosed poles.[52] The integrand of Eq. (21) can be written as

$$A_p(k,\omega) = \frac{N(k,\omega)}{\Delta(k,\omega)}. \quad (25)$$

In Eq. (25), $N(k,\omega) = [P_0'(\alpha_1 r)\Delta_1 + S(\omega)K_0'(\alpha_1 r)\Delta]a\alpha_1$. The poles of the integrand of Eq. (21) correspond to the roots of the dispersion Eq. (9). The denominator and numerator of Eq. (25) are both analytic functions, so the residues of the poles could be computed using the alternative residue formula[50]

$$\text{Residues} = \left.\frac{N(k,\omega)}{\partial\Delta(k,\omega)/\partial k}\right|_{k=k_p}, \quad (26)$$

where k_p is the pth ($p=1,2,3,\ldots$) order root of the dispersion Eq. (9).

Finally, the displacement field in the inner liquid and the pipe due to the contribution of axisymmetric guided modes is

$$u_{r,1} = 2\pi i\sum_p \left.\frac{\alpha_1 aP_0'(\alpha_1 r)\Delta_1}{\partial\Delta/\partial k}\right|_{k=k_p}, \quad (27)$$

$$u_{z,1} = 2\pi\sum_p \left.\frac{kaP_0(\alpha_1 r)\Delta_1}{\partial\Delta/\partial k}\right|_{k=k_p}, \quad (28)$$

$$u_{r,2} = 2\pi i\sum_p \left.\frac{a[\alpha_2 P_0'(\alpha_2 r)\Delta_2 + kP_0'(\beta_2 r)\Delta_3 + \alpha_2 Q_0'(\alpha_2 r)\Delta_4 + kQ_0'(\beta_2 r)\Delta_5]}{\partial\Delta/\partial k}\right|_{k=k_p}, \quad (29)$$

$$u_{z,2} = 2\pi\sum_p \left.\frac{a[kP_0(\alpha_2 r)\Delta_2 + \beta_2 P_0(\beta_2 r)\Delta_3 + kQ_0(\alpha_2 r)\Delta_4 + \beta_2 Q_0(\beta_2 r)\Delta_5]}{\partial\Delta/\partial k}\right|_{k=k_p}. \quad (30)$$

III. NUMERICAL RESULTS AND ANALYSES

A. Dispersion spectra and mode coupling

As discussed in Sec. II B, the coupling between two groups of axisymmetric guided modes propagating in the liquid cylinder and hollow pipe, respectively, yields longitudinal modes in the liquid-filled pipe. The effect of mode coupling can be clearly observed from the dispersion spectra. Dispersion Eqs. (9), (12), and (13) are numerically calculated, in order to obtain all the real roots which correspond to propagating modes. These roots are then traced as a set of dispersion curves, e.g., curves in Fig. 2(a). Our numerical results correlate well with the reference solutions found in Sinha *et al.*[37] Moreover, using the model from Berliner and Solecki,[39,40] which can be applied for isotropic and TI cylinders, to calculate the theoretical dispersion curves obtained in this paper, leads to similar results. Same observation can be obtained using the Disperse software.[53]

In order to provide an illustrative example, we consider a steel pipe filled with water. The longitudinal bulk velocity and density of water are taken to be $V_f = 1500$ m/s and $\rho_1 = 1000\,\text{kg/m}^3$; for the steel pipe, the longitudinal, shear bulk

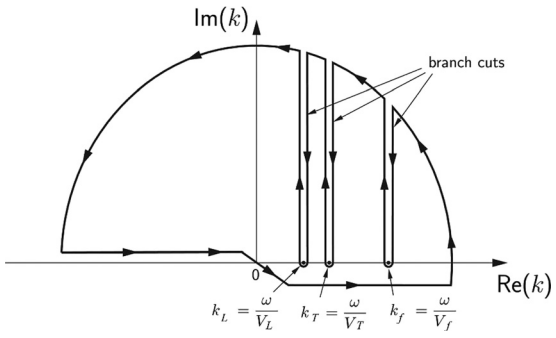

FIG. 1. The contour of integration in Eq. (21).

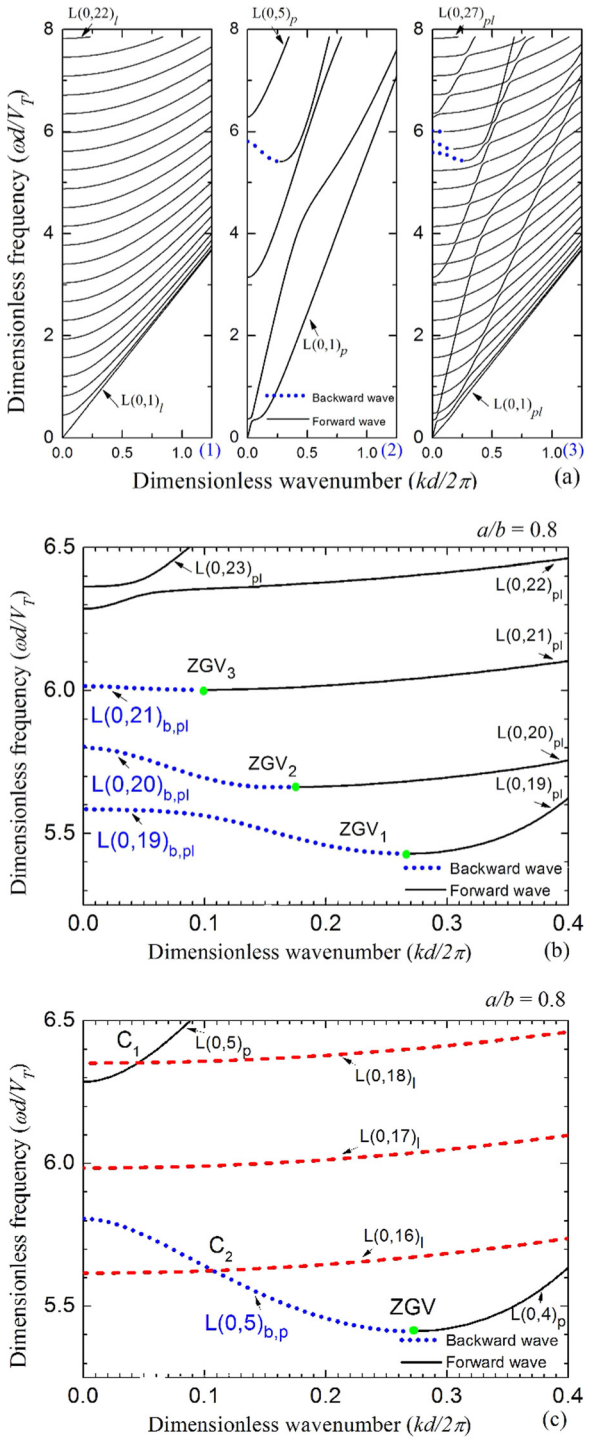

FIG. 2. (Color online) (a) Dispersion spectra of the three groups of axisymmetric longitudinal modes in the water cylinder, in the hollow pipe, and in the steel pipe filled with water, respectively, in the dimensionless frequency range $\omega d/V_T < 8$. In the dimensionless frequency range $5.25 \leq \omega d/V_T \leq 6.5$ and in the Gazis normalized wavenumber range $kd/2\pi \leq 0.4$, dispersion curves of longitudinal modes in the water-filled pipe are presented in (b), and two sets of dispersion curves of modes in the water cylinder and in the hollow pipe, respectively, are given in (c). The internal and external radii of the pipe are $a = 8$ mm and $b = 10$ mm. The vertical and horizontal axes are dimensionless frequency $\omega d/V_T$ and wavenumber $kd/2\pi$, where ω is the angular frequency, d and V_T are the thickness and the shear bulk velocity of the pipe, and k is the wavenumber. Solid lines in (a) and (b) denote forward propagating modes. In (c), the dashed and solid lines represent forward propagating modes in the water cylinder and in the hollow pipe, respectively. Dotted lines in the three figures denote backward propagating modes, and the green dots denote the ZGV points.

velocities, and density are $V_L = 5900$ m/s, $V_T = 3200$ m/s, and $\rho_2 = 7900$ kg/m^3, and its internal and external radii are $a = 8$ mm and $b = 10$ mm. The density ratio is $\rho_1/\rho_2 = 0.13$. Dispersion spectra of longitudinal modes in the liquid cylinder, in the hollow pipe, and in the liquid-filled pipe are presented in the three parts of Fig. 2(a), respectively.

This paper follows the mode classification by Meitzler[54] and Marston.[33] For instance, as labeled in Fig. 2, the longitudinal modes which are forward propagating in the liquid cylinder, pipe, and liquid-filled pipe are denoted as $L(0,m)_l$, $L(0,m)_p$, and $L(0,m)_{lp}$, respectively; where L represents the axisymmetric longitudinal mode with circumferential order $n = 0$, the mode order $m = 1, 2, 3, ...$, and the subscripts l, p, and pl identify three models. The fundamental modes (i.e., those propagating at zero frequency) are given the value by $m = 1$, and the higher order modes are numbered consecutively.

As shown in Fig. 2(a), in the dimensionless frequency range $\omega d/V_T < 8$, 27 longitudinal modes $L(0,m)_{pl}$ ($m = 1,2,\ldots,27$) in the liquid-filled pipe can be decoupled into 22 modes $L(0,m)_l$ ($m = 1,2,\ldots,22$) in the liquid cylinder and 5 modes $L(0,m)_p$ ($m = 1,2,\ldots,5$) in the hollow pipe. The dotted lines in Fig. 2 denote the portions of spectra representing backward waves. In the middle of Fig. 2(a), there is one backward wave in the hollow pipe, while in the right of Fig. 2(a), there are three backward waves in the liquid-filled pipe. Each exists in a narrow frequency range.

For clarity, in Figs. 2(b) and 2(c), we present a zoomed view of the relevant portion of the spectra, showing dispersion curves in the dimensionless frequency range $5.25 \leq \omega d/V_T \leq 6.5$ and in the Gazis normalized wavenumber range $kd/2\pi \leq 0.4$, where $d = b - a$ is the wall thickness of the pipe. These graphs illustrate the effects of coupling between backward and forward modes. Two sets of dispersion curves of guided modes propagating in the liquid cylinder and hollow pipe, respectively, are plotted together in Fig. 2(c), and dispersion curves in the liquid-filled pipe are drawn in Fig. 2(b) for comparisons. The dotted lines represent backward modes, and the green dots denote ZGV points. The ZGV frequencies correspond to the points where the slopes of dispersion curves are zero (i.e., zero group-velocity) and the wavenumbers k are non-zero. They often appear in the vicinity of $k = 0$. And they can be estimated from dispersion spectra or group velocity dispersion curves.

The backward mode propagating in the hollow pipe, $L(0,5)_{b,p}$, is classified as part of the $L(0,5)_p$ mode and is indeed connected to the $L(0,5)_p$ mode through a small imaginary loop in the complex wavenumber space.[1,33] The subscript b denotes backward wave. Backward modes propagating in the liquid-filled pipe are denoted as $L(0,19)_{b,pl}$, $L(0,20)_{b,pl}$, and $L(0,21)_{b,pl}$, respectively. In the real wavenumber plane, the backward $L(0,19)_{b,pl}$ mode is connected with the forward $L(0,19)_{pl}$ mode by the ZGV_1 point. In this paper, only the propagating modes with real wavenumbers are considered. It will be interesting to study the purely imaginary loops of dispersion spectra, e.g., by applying the Newton-Raphson method to find imaginary roots of the dispersion Eq. (9). The aim is to clearly understand how the modes are coupled and how to classify a backward mode with a proper

mode order m. Furthermore, the evanescent branches of dispersion spectra could be studied, e.g., by using the Muller method to calculate complex roots of the Eq. (9), to mark the ZGV points.

For a hollow cylinder, at cutoff frequencies (i.e., the wavenumber $k=0$), guided modes decoupled into pure compressional P modes and pure transverse S modes. For the wavenumber $k \neq 0$, the coupling between compressional P and transverse S type vibrations, which is caused by the boundary conditions, causes repulsions between neighboring dispersion curves of a given symmetry (i.e., the same circumferential number n).[35,55] The repulsion prevents the neighboring dispersion curves from intersecting at $k \neq 0$. The strength of repulsion is related to the frequency separation at $k=0$ between two neighboring modes. The rule is that the smaller the frequency separation at $k=0$, the stronger the repulsion becomes.[14,35] In the vicinity of $k=0$, the strong repulsion between a pair of adjacent P and S waves may yield a backward wave which possesses only one ZGV point.[14,35] For instance, as shown in Fig. 2(c), in the steel pipe, $L(0,5)_{b,p}$ is a backward propagating branch which is caused by the strong coupling between the P and S waves, i.e., $L(0,4)_p$ and $L(0,5)_p$ modes. In the complex wavenumber spectra, the upper threshold of the backward $L(0,5)_{b,p}$ mode and the lower threshold of the forward $L(0,5)_p$ mode are connected by a loop for which the wavenumber k is purely imaginary.[1] The dispersion curve of $L(0,5)_{b,p}$ starts from its dimensionless cutoff frequency of 5.806 at which the wavenumber $k=0$ and the group velocity $V_g = 0$. The dispersion curve proceeds with a negative slope as k increases; and it ends at the ZGV point at 5.411 at which the Gazis normalized wavenumber $kd/2\pi \approx 0.27$ and $V_g = 0$.

In a liquid cylinder, there will be neither a backward wave nor a ZGV point since only P waves exist. For example, as shown in Fig. 2(c), slopes of the three dispersion curves are always positive, i.e., $L(0,16)_l$, $L(0,17)_l$, and $L(0,18)_l$ modes in the water cylinder are forward modes.

The coupling effect can be observed. Dispersion spectra in Figs. 2(b) and 2(c) are similar. The visible difference is that there are two intersections between the two sets of curves at points C_1 and C_2 in Fig. 2(c), while there is no intersection but small gaps next to the near cross-over points in Fig. 2(b). Far from the intersection points, the contribution of the second term of the dispersion Eq. (10) is relatively small compared to that of the first term. That is, the decoupled dispersion Eq. (14) is available, which means that the effects of coupling are weak. However, in the vicinity of an intersection point, the contribution of the second term could not be ignored; in this case, the strong coupling applies.

The strong coupling between two sets of modes in the liquid cylinder and in the hollow pipe, respectively, causes repulsions between neighboring dispersion curves of modes that prevent them from intersecting. There are two types of intersections in Fig. 2(c). One type is that two forward modes intersect at the point C_1; and the other type is that the intersection between the forward and backward modes at point C_2. For the first type, considering the intersection between $L(0,18)_l$ and $L(0,5)_p$ at point C_1 in Fig. 2(c), the strong coupling causes a gap between $L(0,22)_{pl}$ and $L(0,23)_{pl}$ in Fig. 2(b). These modes are still two forward modes which dispersion curves have positive slopes.

We are interested in the second type that is the intersection between backward and forward modes. Next to the intersection point C_2 in Fig. 2(c), the strong coupling between the forward $L(0,16)_l$ and backward $L(0,5)_{b,p}$ modes causes a strong repulsion, which yields a gap between the $L(0,19)_{b,pl}$ and $L(0,20)_{b,pl}$ modes. These modes are two backward modes with negative slopes. Besides, though there is no intersection between the backward $L(0,5)_{b,p}$ and forward $L(0,17)_l$ modes, the effect of repulsion on the forward $L(0,17)_l$ mode is still strong enough to produce the origination of another new backward mode $L(0,21)_{b,pl}$ in the liquid-filled pipe.

As shown in Fig. 2(b), dispersion spectra of the three backward modes $L(0,19)_{b,pl}$, $L(0,20)_{b,pl}$, and $L(0,21)_{b,pl}$ all start from the vertical axis ($k=0$), and end at ZGV points ZGV_1, ZGV_2, and ZGV_3 at dimensionless frequencies 5.427, 5.663, and 6.002, respectively. In the hollow pipe, the ZGV point of the $L(0,5)_{b,p}$ mode appear at 5.411. Clearly, the repulsions among $L(0,5)_{b,p}$, $L(0,16)_l$, and $L(0,17)_l$ modes also cause shifts of frequencies at which ZGV points appear.

In general, the major influences of the water contained in this thin-walled pipe with its radius ratio $a/b=0.8$ are (i) the increased number of backward modes and ZGV points, and (ii) shifts of frequencies corresponding to ZGV points. Furthermore, the water also changes the group velocity dispersion spectrum and the frequency range of existence of a backward mode in the pipe.

B. Influence of the pipe's radius ratio

According to Cui *et al.*,[35] in a hollow pipe, the existence and dispersion property of a backward mode depends not only on Poisson's ratio, but also on the ratio of the inner to the outer radius. In a liquid-filled pipe, this radius ratio also affects the number and distributions of backward waves and ZGV points.

In this section, the dispersion properties of backward waves and ZGVs in pipes of different radius ratios a/b are considered. The material properties of water and steel pipes are the same as those of the example in Sec. III A. The external radius is fixed as $b=10$ mm, and a/b varies from 0.1 to 0.98. Dispersion spectra of longitudinal modes propagating in the water cylinders, hollow steel pipes, and water-filled pipes with $a/b=0.4$, 0.5, and 0.9, respectively, are displayed in Fig. 3. Only modes in the dimensionless frequency range $5.25 \leq \omega d/V_T \leq 6.5$ are given in Fig. 3, in order to focus on the illustration of the influence of a/b.

As shown in Fig. 3, the influence of contained water on the backward modes and ZGVs in a thin-walled pipe with a large a/b is demonstrably greater than that in a thick-walled pipe with a small a/b. As illustrated in Fig. 3(a), for the thick-walled pipe with $a/b=0.4$, there is one backward mode $L(0,5)_{b,p}$ and one associated ZGV point at $\omega d/V_T = 5.565$. As shown in Fig. 3(b), in the water-filled pipe, there is also only one backward mode $L(0,7)_{b,pl}$ which possesses one ZGV point at 5.594. Though the $L(0,7)_{b,pl}$ mode in the

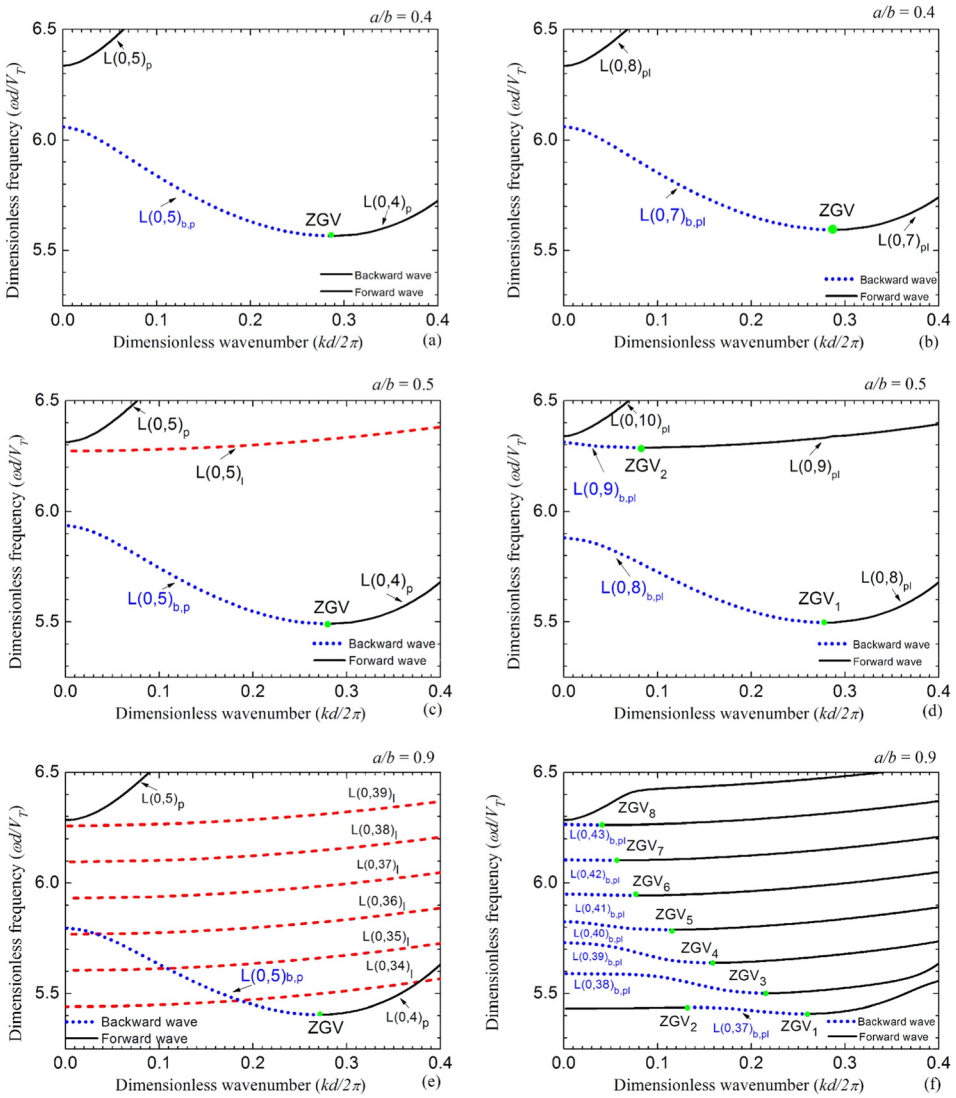

FIG. 3. (Color online) Dispersion spectra of longitudinal modes in the water cylinders with radius $a = 4$, 5, and 9 mm and in the hollow steel pipes with ratios of internal to external radius (a) $a/b = 0.4$, (c) $a/b = 0.5$, and (e) $a/b = 0.9$; and those in the water-filled pipes with (b) $a/b = 0.4$, (d) $a/b = 0.5$, and (f) $a/b = 0.9$. In (a), (c), and (e), dashed and solid lines represent forward propagating modes in the water cylinders and in the hollow pipes, respectively; and dotted lines denote backward modes. In (b), (d), and (f), solid and dotted lines represent forward and backward modes, respectively. The ZGV points are marked by green dots.

liquid-filled pipe has a different mode order (i.e., $m = 7$) from that of the $L(0,5)_{b,p}$ mode in the hollow pipe (i.e., $m = 5$), these two modes have similar dispersion properties (e.g., similar cutoff frequencies and similar frequency ranges in which the two modes exist). In this thick-walled pipe, the contained water does not change the number of the backward mode and ZGV point exhibiting in the fixed frequency range chosen; while it does cause a shift of the frequency corresponding to the ZGV point, which is $\omega d/V_T = 0.029$. In the case of $a/b = 0.5$ as in Fig. 3(d), the inclusion of the water generates two backward modes $L(0,8)_{b,pl}$ and $L(0,9)_{b,pl}$ and two associated ZGVs. For $a/b = 0.9$, as shown in Fig. 3(f), the inclusion of the water causes the generation of seven backward modes $L(0,m)_{b,pl}$ ($m = 37$, 40,…,43) and eight ZGVs. Here, the backward mode $L(0,37)_{b,pl}$ has two ZGV points, ZGV_1 and ZGV_2. At these two ZGV points, the $L(0,37)_{b,pl}$ mode has zero group velocity but non-trivial wave-numbers. This interesting phenomenon of double-ZGVs in a single mode is discussed further below.

Mode coupling can be used to explain why the contained liquid has a major impact on ZGVs in a thin-walled pipe. The coupling strength (i.e., repulsion force) is proportional to the frequency gap between the cutoff and ZGV frequencies of dispersion curves for the liquid column and the hollow cylinder, respectively. In the dimensionless frequency range $\omega d/V_T \leq 8$, cutoff frequencies of longitudinal modes in water columns with radii $a = 1$, 2,…, 9, and 9.5 mm, respectively, and ZGV frequencies of backward modes $L(0,5)_{b,p}$ in hollow steel cylinders with the same external radius $b = 10$ mm and varied inner radii $a = 1$, 2,…, 9, and 9.5 mm, respectively, are plotted in Fig. 4. As shown in Figs. 3(a), 3(c), 3(e), and 4, in the fixed frequency range chosen, the number of longitudinal modes $L(0,m)_l$ in the water cylinder sharply rises with increasing a/b. More intersection points arise and the spacing between the dispersion curves of backward $L(0,5)_{b,p}$ and forward $L(0,m)_l$ modes is reduced. The coupling is strong when a backward mode in the hollow pipe and a forward mode in the liquid cylinder have a narrow frequency-separation, and the strongest coupling corresponds to the case of intersection. The effect of strong coupling is the repulsion, which may generate backward modes and ZGVs. With increasing a/b, the repulsion becomes stronger, so that more backward modes and even more ZGV points appear in the liquid-filled pipe.

Generally, for a thick-walled pipe, the contained water has only a mild effect on the number of backward modes

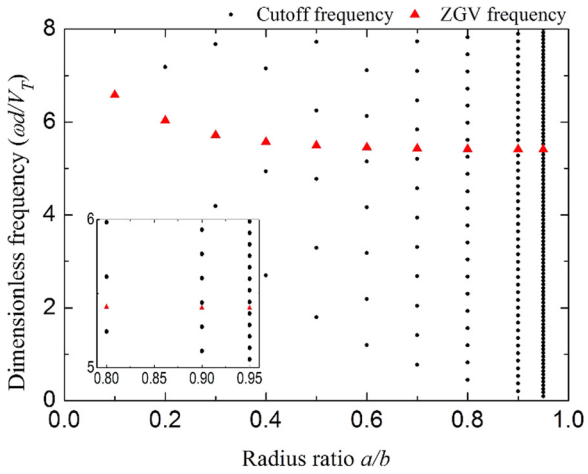

FIG. 4. (Color online) In the dimensionless frequency range $\omega d/V_T \leq 8$, cutoff frequencies of longitudinal modes in the water columns with radii being $a = 1, 2, \ldots, 9$, and 9.5 mm, respectively, are denoted by black dots. And ZGV frequencies of the backward modes $L(0,5)_{b,p}$ in hollow steel pipes with the same outer radius $b = 10$ mm and inner radii being $a = 1, 2, \ldots, 9$, and 9.5 mm, respectively, are denoted by red triangles.

and ZGVs. While in the case of a thin-walled pipe, the presence of water can significantly increase the number of backward modes and ZGVs, and notably, it may cause the phenomenon of double-ZGVs in a single backward mode.

C. Backward wave with double ZGVs

In a hollow pipe, one backward mode possesses only one ZGV at the lowest frequency of the mode. However, in a pipe filled with liquid, under certain conditions, e.g., if the radius ratio a/b of the pipe approaches unity, some backward modes possess double ZGVs. For example, in the water-filled pipe with $a/b = 0.9$ in Fig. 3(f), the slope of the dispersion curve of the backward mode $L(0,37)_{b,pl}$ changes its sign twice at points ZGV_1 and ZGV_2.

In fact, it is found that the phenomenon of double ZGVs is not rare. For example, in the water-filled pipe with $a/b = 0.95$, the strong repulsion between the backward mode $L(0,5)_{b,p}$ in the hollow pipe and the 12 forward modes $L(0,66)_l, \ldots, L(0,77)_l$ in the water cylinder generates 12 backward modes and 15 ZGVs. The first three backward modes $L(0,72)_{b,pl}$, $L(0,73)_{b,pl}$, and $L(0,74)_{b,pl}$ are the double-ZGVs type, as illustrated in Fig. 5. All the other 9 higher order backward modes $L(0,75)_{b,pl}, \ldots, L(0,83)_{b,pl}$ belong to the single-ZGV type. Figures 5(a) and 5(b), respectively, show dispersion spectra and group velocity dispersion curves of the three double-ZGVs backward modes, and the six ZGV points, $ZGV_1 \ldots ZGV_6$. Dotted lines in Fig. 5 represent backward waves. The group velocity is calculated using the relation with phase velocity, as $V_g = V[1 - (\omega/V)(dV/d\omega)]^{-1}$. As illustrated in Fig. 5(b), each backward mode exists in a narrow frequency range which is bordered by two ZGV points, and it has negative group velocities.

In practice, most pipelines that are transmitting liquid are designed to have large inner radii and relatively thin thicknesses for reasons of cost. The existence of backward modes with double-ZGVs is common. In order to provide an illustration, we consider a typical oil pipeline of internal and external

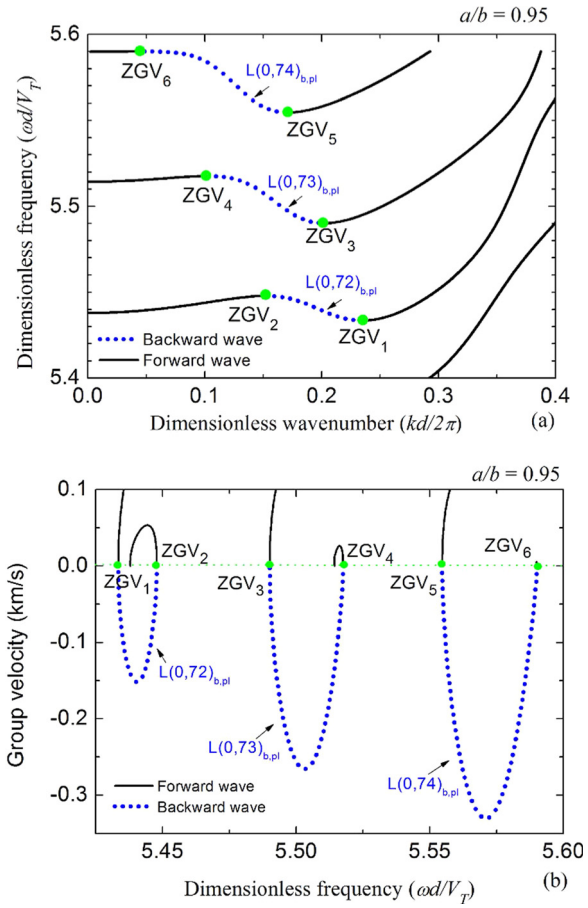

FIG. 5. (Color online) (a) Dispersion spectra and (b) group velocity dispersion curves of the three backward modes in the steel pipe filled with water. Each backward mode has two ZGV points. The inner and outer radii of the pipe are $a = 9.5$ mm and $b = 10$ mm. The dotted and solid lines represent backward and forward modes, respectively. The green dots denote ZGV points.

radii 482 and 508 mm, respectively. The longitudinal bulk velocity and density of the oil are 1290 m/s and 800 kg/m^3; and the longitudinal and shear bulk velocities, and density of the stainless steel pipe are 5980 m/s, 3300 m/s, and 7800 kg/m^3, respectively. From numerical results, it is found that the strong coupling between the backward mode $L(0,5)_{b,p}$ in the hollow steel pipe and the 13 forward propagating longitudinal modes in the oil cylinder produces 13 backward modes and 17 ZGV points in the oil pipe. Moreover, the first four backward modes belong to the double-ZGVs type.

D. Influence of the density ratio

In this section, the influence of the density ratio ρ_1/ρ_2 on the coupling strength is investigated. Considering the thin-walled steel pipe with $a/b = 0.9$ as an illustration, material properties of the pipe and the fluid are the same as those in Fig. 3(f), and the only variable is the fluid density. The steel density is $\rho_2 = 7900$ kg/m^3, and the fluid density ρ_1 varies from 10 to 11 000 kg/m^3, i.e., the density ratio ρ_1/ρ_2 changes from 0.0013 to 1.39. Dispersion spectra of longitudinal modes in fluid columns with different ρ_1, in the hollow pipe, and in fluid-filled pipes with different density

ratios ρ_1/ρ_2 are numerically simulated, respectively. Typical results are given in Fig. 6.

For a fluid column, the secular Eq. (12), i.e., $\Delta_l(V_f, \omega, k) = 0$, is the function of the fluid velocity V_f. It is irrelevant to the fluid density ρ_1, if V_f is assumed to be independent of ρ_1. Hence, in the range $\omega d/V_T \leq 8$, forward modes $L(0,m)_l$ (m = 1,2,..,48) for fluid columns of different densities correspond to the same dispersion spectra, as presented in Fig. 6(a). Similarly, for a hollow cylinder, the secular Eq. (13) $\Delta_p(V_L, V_T, \omega, k) = 0$, that is the function of bulk velocities V_T and V_L, is independent of the cylinder density ρ_2. Dispersion spectra of the forward modes $L(0,m)_p$ (m = 1,2,…,5) and the backward mode $L(0,5)_{b,p}$ are given in Fig. 6(b). The slopes of the two straight lines in Fig. 6(b) are equal to 2π and $2\pi V_L/V_T$, respectively.

For a fluid-filled cylinder, the density ratio ρ_1/ρ_2 does not affect the first term of the secular Eq. (10), i.e., the decoupling term that is the product of two secular equations Δ_l and Δ_p. However, it does affect the second term (the coupling term), as it appears in the matrix element $M_{21} = -\rho_1 a^2 \omega^2 P_0(\alpha_1 a)/\rho_2 V_T^2$. For instance, dispersion spectra of $L(0,m)_{pl}$ (m = 1,2,…,53) modes corresponding to $\rho_1/\rho_2 = 0.013$, 0.253, and 1.14 are given in Figs. 6(c), 6(d), and 6(e), respectively. Slopes of three straight lines (dashed lines) in Figs. 6(c)–6(e) are $2\pi V_f/V_T$, 2π, and $2\pi V_P/V_T$. Here, $V_P = 2V_T\sqrt{1 - V_T^2/V_L^2} \approx 5377$ m/s is the plate velocity. In Fig. 6(c), for the small density ratio $\rho_1/\rho_2 = 0.013$, the coupling strength is weak. The contribution of the guided modes propagating in the hypothetical fluid column can be almost perfectly separated from those propagating in the solid cylinder. In Fig. 6(d), for $\rho_1/\rho_2 = 0.253$, the coupling strength is stronger than that in Fig. 6(c). The decoupling model provided in this paper is still available. That is, if the small gaps between neighboring dispersion curves of $L(0,m)_{pl}$ in Fig. 6(d) are linking together, dispersion curves of $L(0,m)_p$ in Fig. 6(b) can be observed. In Fig. 6(e), for $\rho_1/\rho_2 = 1.14$, the coupling strength is strong, and the decoupling model is not available.

The coupling strength, which is related to the density ratio, clearly affects the number and distribution of backward modes in fluid-filled pipes, as shown in Figs. 6(c), 6(d), and 6(e). For clarity, we present a zoomed view of the relevant portion of the spectra, shown dispersion curves in the dimensionless frequency range $5.25 \leq \omega d/V_T \leq 6.5$ and in the dimensionless wavenumber range $kd/2\pi \leq 0.4$. Dispersion spectra corresponding to ρ_1 = 10, 100, 200, 500, 2000, and 9000 kg/m^3 are given in Figs. 7(a)–7(f), respectively. Numbers of backward modes, backward modes with double-ZGVs, and ZGV points corresponding to different densities ρ_1 in the range $5.25 \leq \omega d/V_T \leq 6.5$ are listed in Table I.

In Fig. 7(a), for $\rho_1/\rho_2 \approx 0.0013$, the coupling strength is quite weak. This weak coupling between the backward mode $L(0,5)_{b,p}$ and the forward modes $L(0,34)_l$, $L(0,35)_l$, and $L(0,36)_l$ generates four backward modes $L(0,m)_{b,pl}$ (m = 37,…,40) and six ZGV points. The $L(0,37)_{b,pl}$ and $L(0,38)_{b,pl}$ exhibit two ZGV frequencies on the same branch. The frequency-gaps between the neighboring backward modes are quite small. If we ignore these small gaps and link the four backward modes, the linked dispersion curve almost coincides with the dispersion curve of the $L(0,5)_{b,p}$ mode in Fig. 3(e).

In Fig. 7(b), for $\rho_1/\rho_2 \approx 0.013$, the coupling strength is relatively stronger than that in Fig. 7(a). Four backward modes $L(0,m)_{b,pl}$ (m = 37,…,40) and 6 ZGV points are generated, and the gaps between neighboring backward modes are relatively larger. The repulsion between two forward modes $L(0,5)_p$ and $L(0,39)_l$ produces the backward mode $L(0,43)_{b,pl}$ and the associated ZGV, i.e., the point z7 in Fig. 7(b).

The coupling strength (repulsion) becomes stronger with increasing density ratio. As shown in Figs. 7(c) and 7(d), the strong repulsion generates more backward modes and ZGV points. However, as listed in Table I, numbers of backward modes and ZGVs do not monotonically increase with increasing ρ_1/ρ_2.

The transition from two ZGV points to one ZGV point on the same branch can be observed with increasing ρ_1/ρ_2. In Figs. 7(a)–7(d), $L(0,37)_{b,pl}$ and $L(0,38)_{b,pl}$ exhibit double-ZGVs. In Fig. 7(e), for $\rho_1/\rho_2 \approx 0.253$, only $L(0,37)_{b,pl}$ exhibits two ZGV frequencies. In Fig. 7(f), for $\rho_1/\rho_2 \approx 1.14$,

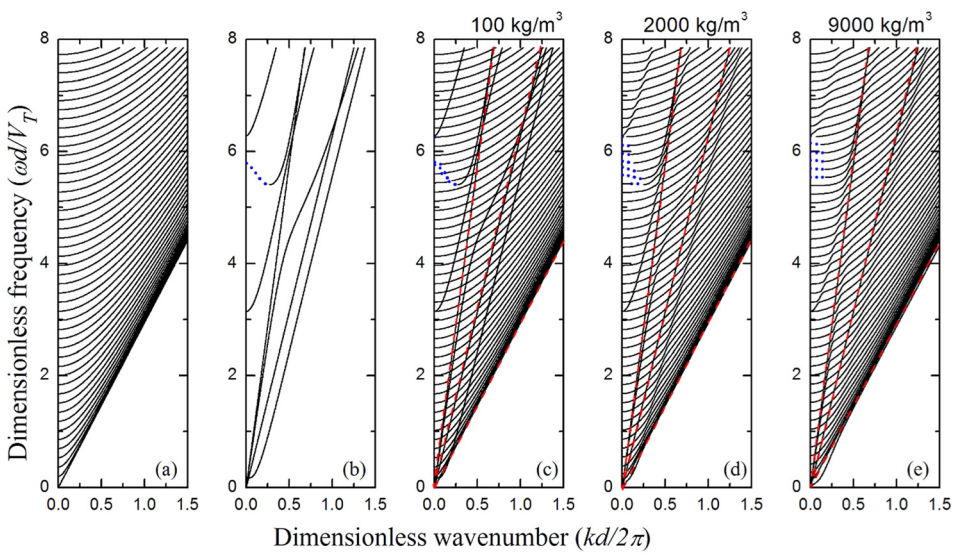

FIG. 6. (Color online) Dispersion spectra of longitudinal modes (a) in the fluid column, (b) in the hollow steel pipe, (c) in the fluid-filled pipes with fluid densities being 100 kg/m^3, (d) 2000 kg/m^3, and (e) 9000 kg/m^3, respectively. Dotted lines denote backward modes.

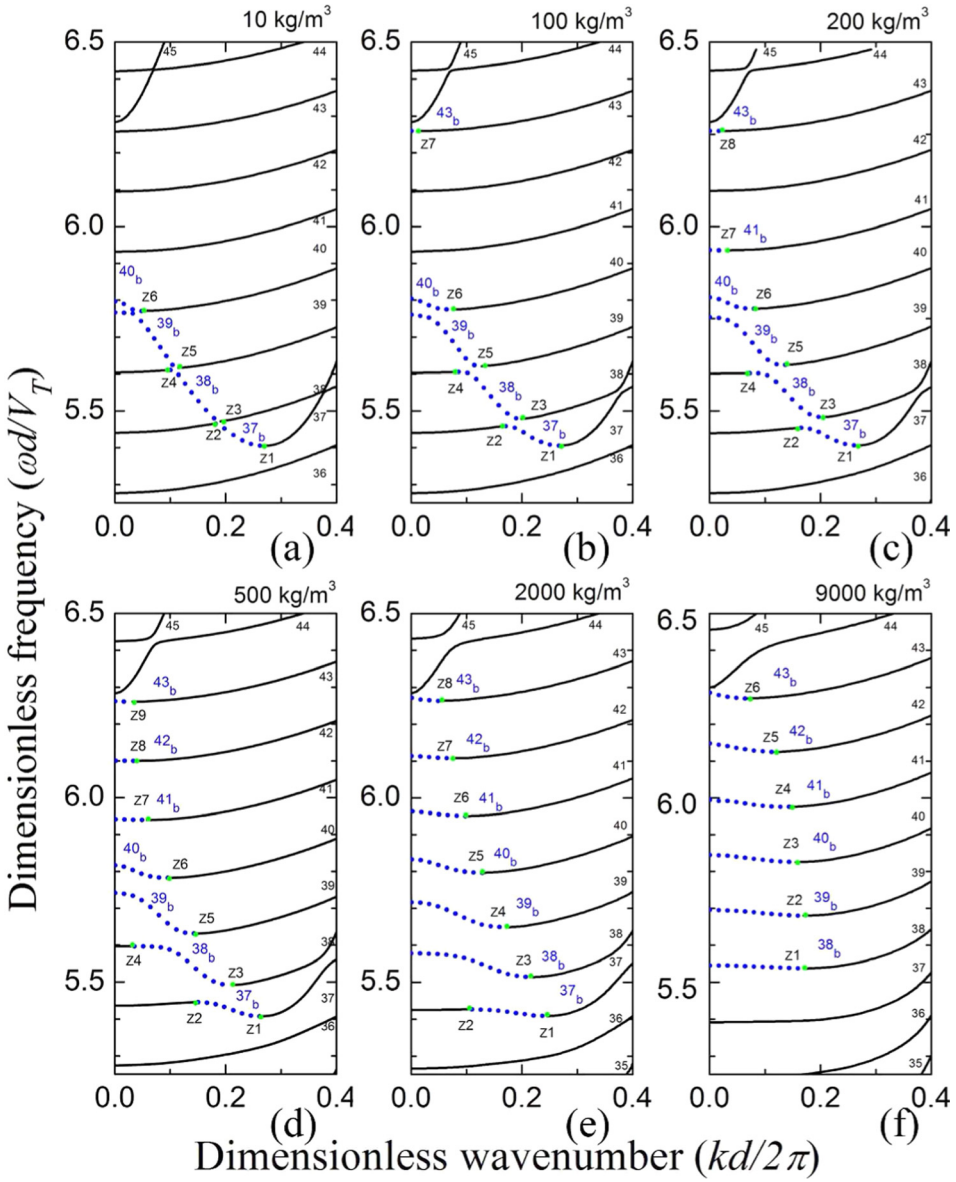

FIG. 7. (Color online) Dispersion spectra of longitudinal modes in fluid-filled pipes of fluid densities $\rho_1 = 10$, 100, 200, 500, 2000, and 9000 kg/m^3 are given in (a) to (f), respectively. For instance, the number 36 denotes $L(0,36)_{pl}$, and the number 37_b denotes $L(0,37)_{b,pl}$. The ZGV points are marked by green dots. The dashed and solid lines represent backward and forward modes, respectively.

none of the six backward modes $L(0,m)_{b,pl}$ ($m = 38,\ldots,43$) exhibits two ZGVs. The reason is that the larger the density ratio ρ_1/ρ_2, the stronger the coupling strength (i.e., repulsion force). For example, in Fig. 7(e), if the repulsion between $L(0,39)_{b,pl}$ and $L(0,38)_{b,pl}$ is strong enough, it leads to the transition from two ZGVs to one ZGV on the lower branch (i.e., the $L(0,38)_{b,pl}$ mode). Moreover, the strong repulsion could cause the disappearance of a backward mode. For example, the $L(0,37)_{b,pl}$ in Fig. 7(e) is a backward mode, while the $L(0,37)_{pl}$ in Fig. 7(f) is a forward mode.

TABLE I. Numbers of backward modes (BW), ZGV points, and backward modes with D-ZGV in fluid-filled pipes of different fluid densities ρ_1.

Density ρ_1 (kg/m^3)	BW	*D*-ZGV	ZGV
10	4	2	6
50	4	2	6
100	5	2	7
200	6	2	8
500	7	2	9
1000	7	1	8
1500	7	1	8
2000	7	1	8
9000	6	0	6
11 000	6	0	6

Particularly, the strong coupling between a forward mode in the hollow cylinder and a forward mode in the hypothetical fluid column could also produce a backward mode. For instance, we present a zoomed view of the relevant portion of the spectra in Fig. 6, shown dispersion curves in the dimensionless frequency range $3.14 \leq \omega d/V_T \leq 3.16$ and in the dimensionless wavenumber range $kd/2\pi \leq 0.05$. Dispersion curves of the forward mode $L(0,19)_l$ in the fluid column and the forward mode $L(0,3)_p$ in the hollow cylinder are given in Fig. 8(a). Spectra corresponding to $\rho_1 = 10$, 100, 9000, and 11 000 kg/m^3 are given in Figs. 8(b)–8(e), respectively.

In Fig. 8(a), two forward modes $L(0,19)_l$ and $L(0,3)_p$ have similar cutoff frequencies and an intersection point in the vicinity of $k = 0$. In Fig. 8(b), for $\rho_1/\rho_2 \approx 0.0013$, the

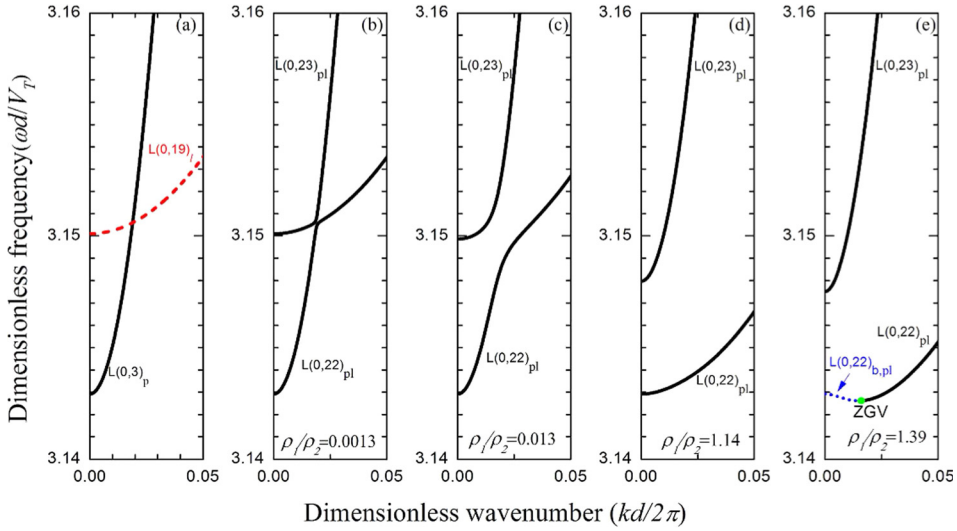

FIG. 8. (Color online) Dispersion spectra of the $L(0,19)_l$ mode in the liquid column and the $L(0,3)_p$ mode in the hollow cylinder with radius ratio $a/b = 0.9$ (a). Dispersion spectra of the $L(0,22)_{pl}$ and $L(0,23)_{pl}$ modes in fluid-filled pipes with density ratios (b) $\rho_1/\rho_2 \approx 0.0013$, (c) $\rho_1/\rho_2 \approx 0.013$, (d) $\rho_1/\rho_2 \approx 1.14$, and (e) $\rho_1/\rho_2 \approx 1.39$, respectively.

weak coupling generates a small gap between curves of two forward modes $L(0,22)_{pl}$ and $L(0,23)_{pl}$. In Figs. 8(c) and 8(d), with increasing density ratio ρ_1/ρ_2, the coupling strength (repulsion force) is stronger, the gap becomes wider, while the separation of two cutoff frequencies of $L(0,22)_{pl}$ and $L(0,23)_{pl}$ becomes narrower. In Fig. 8(e), for $\rho_1/\rho_2 \approx 1.39$, the strong repulsion generates a backward propagating region in the lower branch, i.e., the backward mode $L(0,22)_{b,pl}$.

E. Excitation intensity properties

It is assumed that an axisymmetric point source model is placed at the origin of the cylindrical coordinate system of a liquid-filled pipe, and only axisymmetric longitudinal modes ($n = 0$) are excited. Amplitude spectra of longitudinal modes, including backward and forward modes, excited by the point source are numerically calculated using Eqs. (27)–(30). The objective is to explore the excitation properties of backward waves and ZGV modes.

Typical results of amplitude spectra of backward modes with single-ZGV and double-ZGVs are presented in Figs. 9 and 10, respectively. The solid and dotted lines present amplitudes of forward and backward modes, respectively. Verification of numerical results is achieved by checking that, at the liquid-solid interface $r = a$, the radial displacement components in the liquid are equal to that in the pipe, i.e., the continuous boundary condition $u_{r,1}|_{r=a} = u_{r,2}|_{r=a}$ is satisfied.

We use the complex contour integration and residue method to evaluate the excitation of waveguide modes. This method is widely used in geophysical prospecting in cased holes which can be modeled as fluid-filled cylinders.[37,50] And it can provide conceptual tools in the isolation of the contribution of specific modes of wave propagation to the composite waveform. Other methods, for example, the method from Auld[56] (modal analysis), which is commonly used for analyses of excitation of guided modes in plates,[57] leads to similar results presented in this paper. For a hypothetical fluid column, it can be theoretically proved that the complex contour integration method and the Auld's method produce the same expressions of displacement components.[58] For a liquid-filled pipe, it will be interesting to theoretically prove that the two methods lead to the similar solutions.

1. Single ZGV point in one backward mode

In the water-filled pipe with $a/b = 0.8$, as shown in Fig. 2(b), slopes of dispersion curves of the three backward modes $L(0,19)_{b,pl}$, $L(0,20)_{b,pl}$, and $L(0,21)_{b,pl}$ only change their signs for once, that is, each mode has a single ZGV point at ZGV_1, ZGV_2, and ZGV_3, respectively.

Absolute values of the axial and radial displacement components of guided modes in the water-filled pipe are denoted u_z and u_r, respectively. The components u_z and u_r of the three backward and 24 forward modes excited by the point source, with the radial distance $r = a = 8$ mm (i.e., at the water-pipe interface), are shown in Figs. 9(a) and 9(b), as functions of frequency in the range $5.4 \le \omega d/V_T \le 6.1$.

For each of the three backward modes, the amplitudes of u_z and u_r are seen to increase dramatically as the ZGV frequency is approached, which implies a highly excitable condition at ZGV_1, ZGV_2, and ZGV_3 (i.e., ZGV resonances). The other significant feature in Fig. 9(b) is that amplitudes of u_r for backward modes also rise sharply as their own cutoff frequencies, i.e., f_{cut1}, f_{cut2}, and f_{cut3}, are approached, respectively (i.e., thickness resonances). While this feature is not present in Fig. 9(a). In fact, the component u_{z1} of each of backward or forward modes needs to be zero at the cutoff frequency. The reason is that, at a mode's cutoff frequency, the wavenumber is zero ($k = 0$), and this appears in the numerator in the Eq. (28) for the calculation of u_{z1}. This relation has been used to verify our numerical results.

In Fig. 9, ZGV resonances at ZGV frequencies and thickness resonances at cutoff frequencies are favorably generated. This can be explained theoretically. For example, the denominator in the Eq. (27), which is the expression of the radial displacement component in the fluid $u_{r,1}$, is $\partial\Delta/\partial k$. It can be expressed as $\partial\Delta/\partial k = (\partial\Delta/\partial\omega)(\partial\omega/\partial k)$, where $\partial\omega/\partial k$ is the group velocity. For each mode, at its cutoff frequency and ZGV frequencies (if exist), its group velocity

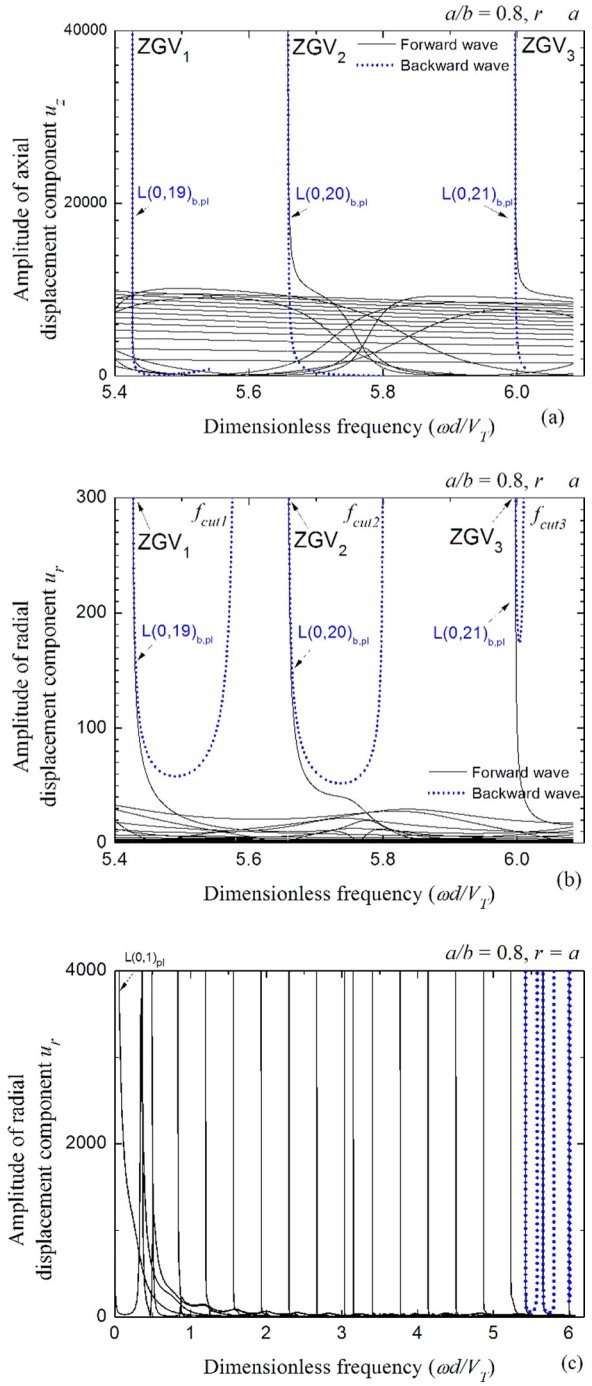

FIG. 9. (Color online) In the water-filled pipe with radius ratio $a/b = 0.8$, amplitude spectra of the axial and radial displacement components, u_z and u_r, of guided modes on the liquid-solid interface in the frequency range $5.4 \le \omega d/V_T \le 6.1$ are given in (a) and (b), respectively. Spectra of u_r in the range $\omega d/V_T \le 6.1$ are given in (c). Each backward mode has a single ZGV point. The dotted and solid lines denote backward and forward modes, respectively.

$V_g = \partial\omega/\partial k$ is equal to zero, and the denominator is equal to zero. Hence, theoretically, amplitudes of $u_{r,1}$ are infinite at cutoff and ZGV frequencies, as shown in Fig. 9(b), which corresponds to thickness and ZGV resonances, respectively. Similar derivations apply to the expression of $u_{r,2}$ in the Eq. (29).

As shown in Fig. 9(c), the dominant mode highly excitable by an axisymmetric point source is the $L(0,1)_{pl}$ mode,

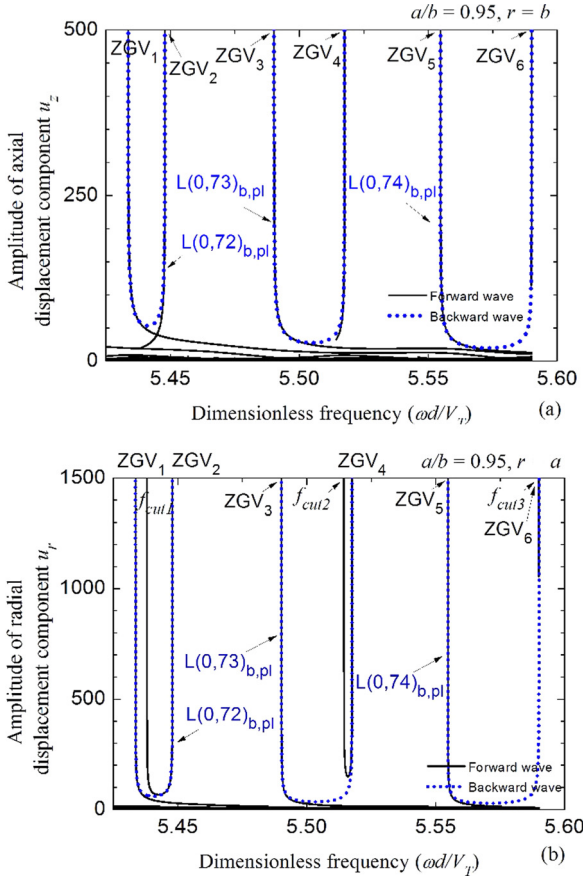

FIG. 10. (Color online) In the water-filled pipe with radius ratio $a/b = 0.95$, amplitude spectra of the axial and radial displacement components of guided modes, i.e., u_z on the external interface $r = b = 10$ mm and u_r on the internal interface $r = a = 9.5$ mm, are given in (a) and (b), respectively. Each backward mode has two ZGV points. The dotted and solid lines denote backward and forward modes, respectively.

which is equivalent to A_0 mode in plates. However, if the excitation frequency is relatively high, as shown in Figs. 9(a) and 9(b), the amplitudes of u_r and u_z for each of the three backward modes in the frequency range in which they exist are orders of magnitude larger than those of the other forward modes. This implies that, in certain frequency ranges, the backward modes are highly excitable by a point source in a liquid-filled pipe.

2. Double ZGV points in one backward mode

We close by considering the excitation properties of a backward mode with double ZGVs, and the water-filled pipe with $a/b = 0.95$ is used for illustration. As displayed in Fig. 5, each of the three backward modes $L(0,72)_{b,pl}$, $L(0,73)_{b,pl}$, and $L(0,74)_{b,pl}$ possesses two ZGV points at the locations marked $ZGV_1 \ldots ZGV_6$ in the figure. Amplitude spectra of the axial and radial displacement components u_z and u_r in the frequency range $5.4 \le \omega d/V_T \le 6.1$ are given in Figs. 10(a) and 10(b), respectively.

In the frequency range $5.4 \le \omega d/V_T \le 6.1$, the amplitudes for the other forward modes studied are orders of magnitude lower than those of the backward modes with double ZGVs, implying an excitable condition for these backward modes. In addition, for each of the three backward modes, the

amplitudes of u_z and u_r both increase dramatically as the frequency approaches the upper and lower bounds of the frequency range in which the mode exists, i.e., the two ZGV frequencies. It means that, at the ZGV frequencies, all these backward modes are highly excitable (i.e., ZGV resonances). As shown in Fig. 10(b), peaks of amplitudes of u_r are also exhibited at the cutoff frequencies of the backward modes (i.e., thickness resonances). Moreover, as discussed in Sec. III C, the water containment in this thin-walled pipe causes three backward modes with double ZGVs and nine backward modes with single ZGV. From numerical results, the other nine backward modes with single ZGV, $L(0,75)_{b,pl}$,…, $L(0,83)_{b,pl}$, and the associated nine ZGV modes are also excitable. Thus, it is possible to excite 15 ZGV resonances using the point source in this thin-walled pipe filled with water.

Generally, for a thin-walled pipe, the inclusion of water can dramatically affect the backward modes. It may cause two types of backward modes with single- or double-ZGV points, greatly increasing the number of ZGV modes. From the analyses of excitation properties, it is concluded that all the ZGVs are highly excitable by the point source, and those ZGV frequencies are usually shifted from the original ZGV frequency in the hollow pipe. That is, it is expected that a number of ZGV resonances will exhibit near the original ZGV frequency. This group of ZGV resonances could increase the intensity of the ZGV signal.

IV. CONCLUSIONS

Generally, for a thick-walled pipe, contained liquid only mildly affects the number of backward waves and ZGV modes. However in the case of a thin-walled pipe, the presence of contained liquid leads to an increased number of backward propagating waves and ZGV modes.

Mode coupling can be used to explain the effect of introducing the liquid. The increased number of backward waves and ZGVs are caused by strong coupling between a backward mode in the hollow pipe and several forward modes in the liquid cylinder. In the dimensionless frequency-wavenumber plane, the strength of repulsion (i.e., coupling) is related to the frequency separation between two dispersion curves of a pair of longitudinal modes propagating, respectively, in the liquid cylinder and in the hollow pipe. The general rule is that the smaller the frequency separation, the stronger the repulsion becomes. The strongest repulsion corresponds to the case of intersection of the dispersion curves for two modes. If the repulsion between a backward mode in the hollow pipe and a forward mode in the liquid cylinder is sufficiently strong, it could produce two backward modes in the liquid-filled pipe, and each of the two backward modes may possess one or two ZGV points.

In a liquid-filled pipe, a backward mode may have two ZGV points. This type of backward mode is often found in a thin-walled pipe having a radius ratio a/b approaching unity. In practical projects, most oil pipelines have a relatively thin-wall compared to the inner and outer radii. Hence, the double-ZGV type of backward mode could be expected to be common. From the excitation analysis, it is concluded that backward modes and ZGVs are highly excitable by a point source which is placed centrally in the liquid-filled pipe. This implies that the ZGV technique has the potential to be applied for in-service inspection of pipelines which are carrying liquid.

In this paper, we have limited our study to longitudinal modes. In practice, if a point source is not perfectly centered (or the circular cylinder is not perfect), then all the mode families, axisymmetric modes longitudinal L(0,m) and torsional T(0,m), and non-axisymmetric flexural modes F(n,m) (n = 1,2,… and m = 1,2,…) are excited. And a high number of F(n,m) modes also exhibit backward branches and ZGV points.[18] According to Ibanescu *et al.*,[55] in a circular waveguide with constant cross-section, there is no interaction between a longitudinal mode and a flexural mode. And due to the continuous rotational symmetry of a fluid-filled pipe, longitudinal and flexural modes are uncoupled for any wavenumber k.[55] Hence, the backward branches of longitudinal modes are not relevant to those of flexural modes. The analyses of mode coupling and excitation of longitudinal backward modes in a fluid-filled cylinder could be extended for analyzing properties of ZGV resonances of flexural modes. Moreover, this peculiar coupling effect of double ZGV points could be also observed both in a viscous liquid and a fluid-filled cylinder immersed in fluid.

ACKNOWLEDGMENTS

This work is supported by the 2009 Newton International Fellowships and Follow-on Support, the National Natural Science Foundation of China with Grants No.11474303 and No. 11134011, the National R&D Projects for Key Scientific Instruments with Grant No. ZDYZ2012-1-07, and the "12th Five-Year Plan" period for informatization project in supercomputing key demonstration, Chinese Academy of Sciences with Grant No. XXH12503-02-02-2 (07).

APPENDIX: MATRIX ELEMENTS OF DISPERSION EQUATION

The dispersion equation of axisymmetric guided waves in a pipe filled with liquid is found by setting to zero the determinant of a 5×5 coefficient matrix, i.e., Eq. (9). The matrix elements are listed using the following notation:

$$v_1 = \alpha_1 a, \quad w_1 = \alpha_2 a, \quad w_2 = \alpha_2 b, \quad x_1 = \beta_2 a,$$
$$x_2 = \beta_2 b, \quad Y_1 = ka, \quad Y_2 = kb,$$

$$M_{11} = v_1 P_0'(v_1),$$
$$M_{12} = w_1 P_0'(w_1),$$
$$M_{13} = Y_1 P_0'(x_1),$$
$$M_{14} = w_1 Q_0'(w_1),$$
$$M_{15} = Y_1 Q_0'(x_1),$$

$$M_{21} = -\rho_1 a^2 \omega^2 P_0(v_1)/\rho_2 V_T^2,$$
$$M_{22} = (2Y_1^2 - a^2\omega^2/V_T^2) P_0(w_1) - 2w_1 P_0'(w_1),$$
$$M_{23} = 2Y_1[x_1 P_0(x_1) - P_0'(x_1)],$$
$$M_{24} = (2Y_1^2 - a^2\omega^2/V_T^2) Q_0(w_1) - 2w_1 Q_0'(w_1),$$
$$M_{25} = 2Y_1[x_1 Q_0(x_1) - Q_0'(x_1)],$$

$$
\begin{aligned}
M_{31} &= 0,\\
M_{32} &= 2w_1Y_1P_0'(w_1),\\
M_{33} &= (Y_1^2 + x_1^2)P_0'(x_1),\\
M_{34} &= 2w_1Y_1Q_0'(w_1),\\
M_{35} &= (Y_1^2 + x_1^2)Q_0'(x_1),
\end{aligned}
$$

$$
\begin{aligned}
M_{41} &= 0,\\
M_{42} &= (2Y_2^2 - b^2\omega^2/V_T^2)P_0(w_2) - 2w_2P_0'(w_2),\\
M_{43} &= 2Y_2[x_2P_0(x_2) - P_0'(x_2)],\\
M_{44} &= (2Y_2^2 - b^2\omega^2/V_T^2)Q_0(w_2) - 2w_2Q_0'(w_2),\\
M_{45} &= 2Y_2[x_2Q_0(x_2) - Q_0'(x_2)],
\end{aligned}
$$

$$
\begin{aligned}
M_{51} &= 0,\\
M_{52} &= 2w_2Y_2P_0'(w_2),\\
M_{53} &= (Y_2^2 + x_2^2)P_0'(x_2),\\
M_{54} &= 2w_2Y_2Q_0'(w_2),\\
M_{55} &= (Y_2^2 + x_2^2)Q_0'(x_2).
\end{aligned}
$$

[1]H. Meitzler, "Backward-wave transmission of stress pulses in elastic cylinders and plates," J. Acoust. Soc. Am. **38**(5), 835–842 (1965).
[2]M. Germano, A. Alippi, M. Angelici, and A. Bettucci, "Self-interference between forward and backward propagating parts of a single acoustic plate mode," Phys. Rev. E **65**, 046608 (2002).
[3]S. Bramhavar, C. Prada, A. A. Maznev, A. G. Every, T. B. Norris, and T. W. Murray, "Negative refraction and focusing of elastic Lamb waves at an interface," Phys. Rev. B **83**, 014106 (2011).
[4]K. Negishi, "Negative group velocities of Lamb waves," J. Acoust. Soc. Am. **64**, S63 (1978).
[5]J. Wolf, T. D. K. Ngoc, R. Kille, and W. G. Mayer, "Investigation of Lamb waves having a negative group velocity," J. Acoust. Soc. Am. **83**(1), 122–126 (1988).
[6]K. Nishimiya, K. Yamamoto, K. Mizutani, and N. Wakatsuki, "Negative group velocities of Lamb-type waves in a glass/water/glass structure controlled by the thickness of water layer," Jpn. J. Appl. Phys. **46**, 4483–4485 (2007).
[7]K. Nishimiya, K. Mizutani, N. Wakatsuki, and K. Yamamoto, "Relationships between existence of negative group velocity and physical parameters of materials for Lamb-type waves in solid/liquid/solid structure," Jpn. J. Appl. Phys. **47**, 3855–3858 (2008).
[8]R. D. Mindlin, "Waves and vibrations in isotropic, elastic plates," in *Structural Mechanics, Proceedings of the First Symposium on Naval Structural Mechanics*, Stanford University, CA, 11–14 August 1958, edited by J. N. Goodier and N. J. Hoff (Pergamon, New York, 1960).
[9]C. Prada, O. Balogun, and T. W. Murray, "Laser-based ultrasonic generation and detection of zero-group velocity Lamb waves in thin plates," Appl. Phys. Lett. **87**, 194109 (2005).
[10]S. D. Holland and D. E. Chimenti, "High contrast air-coupled acoustic imaging with zero group velocity Lamb modes," Appl. Phys. Lett. **83**, 2704–2706 (2003).
[11]A. Gibson and J. Popovics, "Lamb waves basis for impact echo method analysis," J. Eng. Mech. **131**(4), 438–443 (2005).
[12]C. Prada, D. Clorennec, T. W. Murray, and D. Royer, "Influence of the anisotropy on zero-group velocity Lamb modes," J. Acoust. Soc. Am. **126**, 620–625 (2009).
[13]D. Clorennec, C. Prada, and D. Royer, "Local and noncontact measurements of bulk acoustic wave velocities in thin isotropic plates and shells using zero-group velocity Lamb modes," J. Appl. Phys. **101**, 034908 (2007).
[14]C. Prada, D. Clorennec, and D. Royer, "Local vibration of an elastic plate and zero-group velocity Lamb modes," J. Acoust. Soc. Am. **124**, 203–212 (2008).
[15]D. Clorennec, C. Prada, and D. Royer, "Laser ultrasonic inspection of plates using zero-group velocity Lamb modes," IEEE Trans. Ultrason. Ferroelectr. Freq. Control **57**(5), 1125–1132 (2010).
[16]S. Mezil, J. Laurent, D. Royer, and C. Prada, "Non contact probing of interfacial stiffnesses between two plates by zero-group-velocity Lamb modes," Appl. Phys. Lett. **105**, 021605 (2014).
[17]M. Ces, D. Royer, and C. Prada, "Characterization of mechanical properties of a hollow cylinder with zero group velocity Lamb modes," J. Acoust. Soc. Am. **132**(1), 180–185 (2012).
[18]J. Laurent, D. Royer, T. Hussain, F. Ahmad, and C. Prada, "Laser induced zero-group velocity resonances in transversely isotropic cylinder," J. Acoust. Soc. Am. **137**(6), 3325–3334 (2015).
[19]A. A. Maznev and A. G. Every, "Surface acoustic waves with negative group velocity in a thin film structure on silicon," Appl. Phys. Lett. **95**, 011903 (2009).
[20]A. A. Maznev and A. G. Every, "Existence of backward propagating acoustic waves in supported layers," Wave Motion **48**, 401–407 (2011).
[21]M. Ces, D. Clorennec, D. Royer, and C. Prada, "Thin layer thickness measurements by zero group velocity Lamb mode resonances," Rev. Sci. Instrum. **82**, 114902 (2011).
[22]M. J. S. Lowe, D. N. Alleyne, and P. Cawley, "Defect detection in pipes using guided waves," Ultrasonics **36**, 147–154 (1998).
[23]H. Lamb, "On group-velocity," in *Proceedings of the London Mathematical Society* (1904), Vol. 1, pp. 473–479.
[24]I. Tolstoy and E. Usdin, "Wave propagation in elastic plates: Low and high mode dispersion," J. Acoust. Soc. Am. **29**, 37–42 (1957).
[25]R. D. Mindlin and M. A. Medick, "Extensional vibrations of elastic plates," J. Appl. Mech. **26**, 561–569 (1959).
[26]M. A. Biot, "Propagation of elastic waves in a cylindrical bore containing a fluid," J. Appl. Phys. **23**, 997–1005 (1952).
[27]J. L. Tassoulas and T. R. Akylas, "On wave modes with zero group velocity in an elastic layer," J. Appl. Mech. **51**(3), 652–656 (1984).
[28]J. Zemanek, Jr., "An experimental and theoretical investigation of elastic wave propagation in cylinder," doctoral dissertation, University of California, Los Angeles, CA, 1962.
[29]K. Negishi and H. Li, "Strobo-photoelastic visualization of Lamb waves with negative group velocity propagating on a glass plate," Jpn. J. Appl. Phys. **35**, 3175–3176 (1996).
[30]K. Negishi, "Existence of negative group velocities in Lamb waves," Jpn. J. Appl. Phys. **26**, 171–173 (1987).
[31]T. Hussain and F. Ahmad, "Lamb modes with multiple zero-group velocity points in an orthotropic plate," J. Acoust. Soc. Am. **132**(2), 641–645 (2012).
[32]E. Kausel, "Number and location of zero-group-velocity modes," J. Acoust. Soc. Am. **131**(5), 3601–3610 (2012).
[33]P. L. Marston, "Negative group velocity Lamb waves on plates and applications to the scattering of sound by shells," J. Acoust. Soc. Am. **113**(5), 2659–2662 (2003).
[34]G. Kaduchak, D. H. Hughes, and P. L. Marston, "Enhancement of the backscattering of high-frequency tone bursts by thin spherical shells associated with a backwards wave: Observations and ray approximation," J. Acoust. Soc. Am. **96**(6), 3704–3714 (1996).
[35]H. Cui, W. Lin, H. Zhang, X. Wang, and J. Trevelyan, "Characteristics of group velocities of backward waves in a hollow cylinder," J. Acoust. Soc. Am. **135**(6), 3398–3408 (2014).
[36]C. R. Fuller, "Monopole excitation of vibrations in an infinite cylindrical elastic shell filled with fluid," J. Sound Vib. **96**(1), 101–110 (1984).
[37]B. K. Sinha, T. J. Plona, S. Kostek, and S.-K. Chang, "Axisymmetric wave propagation in fluid-loaded cylindrical shells. I: Theory," J. Acoust. Soc. Am. **92**(2), 1132–1143 (1992).
[38]M. V. Predoi, "Guided waves dispersion equations for orthotropic multilayered pipes solved using standard finite elements code," Ultrasonics **54**(7), 1825–1831 (2014).
[39]M. J. Berliner and R. Solecki, "Wave propagation in fluid-loaded, transversely isotropic cylinders. Part I. Analytical formulation," J. Acoust. Soc. Am. **99**, 1841–1847 (1996).
[40]M. J. Berliner and R. Solecki, "Wave propagation in fluid-loaded, transversely isotropic cylinders. Part II. Numerical results," J. Acoust. Soc. Am. **99**, 1848–1853 (1996).
[41]C. R. Fuller and F. J. Fahy, "Characteristics of wave propagation and energy distributions in cylindrical elastic shells filled with fluid," J. Sound Vib. **81**, 501–518 (1982).
[42]R. Kumara and S. Ram, "Flexural vibrations of a fluid-filled cylindrical cavity in an infinite solid medium," Acustica **22**, 163–171 (1969/70).
[43]T. J. Plona, B. K. Sinha, S. Kostek, and S. K. Chang, "Axisymmetric wave propagation in fluid-loaded cylindrical shells. II: Theory versus experiment," J. Acoust. Soc. Am. **92**(2), 1144–1155 (1992).

[44]R. Thurston, "Elastic waves in rods and clad rod," J. Acoust. Soc. Am. **64**(1), 1–37 (1978).
[45]B. N. Pavlakovic, "Leaky guided ultrasonic waves in NDT," Ph.D. thesis, Imperial College of Science, Technology, and Medicine, University of London, London, UK (1998), pp. 37–38.
[46]M. J. S. Lowe, "Matrix techniques for modeling ultrasonic waves in multilayered media," IEEE Trans. Ultrason. Ferroelectr. Freq. Control **42**, 525–542 (1995).
[47]W. H. Press, S. A. Teukolsky, W. T. Vetterling, and B. P. Flannery, *Numerical Recipes in C: The Art of Scientific Computing*, 2nd ed. (Cambridge University Press, New York, 1992), Chap. 9, pp. 362 and 371.
[48]W. J. Jacobi, "Propagation of sound waves along liquid cylinders," J. Acoust. Soc. Am. **21**, 120–127 (1949).
[49]D. C. Gazis, "Three-dimensional investigation of the propagation of waves in hollow circular cylinders, I. Analytical Foundation," J. Acoust. Soc. Am. **31**, 568–572 (1959); "Three-dimensional investigation of the propagation of waves in hollow circular cylinders. II. Numerical results," *ibid.* **31**, 573–577 (1959).
[50]A. L. Kurkjian, "Numerical computation of individual far-field arrivals excited by an acoustic source in a borehole," Geophysics **50**(5), 852–866 (1985).
[51]P. M. Morse and H. Feshbach, *Methods of Theoretical Physics* (McGraw-Hill Book Company, New York, 1953), pp. 52–53.
[52]E. W. Peterson, "Acoustic wave propagation along a fluid-filled cylinder," J. Appl. Phys. **45**(8), 3340–3350 (1974).
[53]B. N. Pavlakovic, M. J. S. Lowe, D. N. Alleyne, and P. Cawley, "DISPERSE: A general purpose program for creating dispersion curves," in *Review of Progress in Quantitative NDE*, edited by D. O. Thompson and D. E. Chimenti (Plenum, New York, 1997), Vol. 16, pp. 185–192.
[54]H. Meitzler, "Mode coupling occurring in the propagation of elastic pulses in wires," J. Acoust. Soc. Am. **33**, 435–445 (1961).
[55]M. Ibanescu, S. G. Johnson, D. Roundy, C. Luo, Y. Fink, and J. D. Joannopoulos, "Anomalous dispersion relations by symmetry breaking in axially uniform waveguides," Phys. Rev. Lett. **92**, 063903 (2004).
[56]B. A. Auld, *Acoustic Fields and Waves in Solids* (Wiley Interscience, New York, 1973), Vol. II, Chap. 10, pp. 156–162.
[57]X. Jia, "Modal analysis of the Lamb wave generation in elastic plates by liquid wedge transducers," J. Acoust. Soc. Am. **101**, 834–842 (1997).
[58]H. Zhang, *Theoretical Acoustics*, Rev. Ed. (Higher Education Press, Beijing, China, 2012), Chap. 8, pp. 356–357 (in Chinese).